05952-H177-R0-00

NATIONAL AERONAUTICS AND SPACE ADMINISTRATION

MSC INTERNAL NOTE NO. 67-FM-50

25 APRIL 1967

# THERMO-STRUCTURAL FAILURE LIMITS FOR THE SPACECRAFT COMPONENTS DURING AN UPRATED SATURN 1 LAUNCH

By APOLLO ENGINEERING OPERATIONS DEPARTMENT,

TRW SYSTEMS

C. D. Faust

A. Gillies

R. G. Posgay

NASA/MSC TASK MONITOR

C. T. HYLE



MISSION PLANNING AND ANALYSIS DIVISION
MANNED SPACECRAFT CENTER
HOUSTON, TEXAS

MSC INTERNAL NOTE NO. 67-FM-50

# THERMO-STRUCTURAL FAILURE LIMITS FOR THE SPACECRAFT COMPONENTS FOR AN APOLLO 1B LAUNCH ENVIRONMENT

By C. D. Faust, A. Gillies, R. G. Posgay
Apollo Engineering Operations Department, TRW Systems

25 APRIL 1967

MISSION PLANNING AND ANALYSIS DIVISION
NATIONAL AERONAUTICS AND SPACE ADMINISTRATION
MANNED SPACECRAFT CENTER
HOUSTON, TEXAS

Approved by C. C. Allen
C. C. Allen, Chief
Contingency Analysis Section
NASA/MSC

Approved by C. R. Hicks Jr.
C. R. Hicks, Jr., Chief
Flight Analysis Branch
NASA/MSC

Approved by J. R. Mayer
J. R. Mayer, Chief
Mission Planning and Analysis Division
NASA/MSC

Approved by A. J. Rinaldi
A. J. Rinaldi, Manager
Apollo Engineering Operations Department
TRW Systems

Approved by J. R. Vail
J. R. Vail, Task Manager
Structures Department
TRW Systems

Approved by Bruce J. Gordon
Bruce J. Gordon, Manager
Systems Analysis and Operations
Mission Trajectory Control Program
TRW Systems

# ABSTRACT

The study was performed under the agreements contained in MSC/TRW Task A-96, Abort Limit Lines Due to Saturn Launch Vehicle and Apollo Spacecraft Structural Constraints, Amendment No. 3, Subtask A-96.10 - Effect of Aerodynamic Heating on Limit Lines.

This study is an analysis of the structural failure limits of the spacecraft components of the Mission AS-204 launch configuration when the effects of aerodynamic heating on structural capability are considered. The study is limited to slow divergence dispersions that are detectable by ground based equipment. Structural loads were computed by the TRW N-Stage Computer Program. Skin temperatures were computed using the TRW Ascent Heating Program which was developed for use in this task.

CONTENTS

# FIGURES

# 1. INTRODUCTION AND SUMMARY

## 1.1 INTRODUCTION

The object of this study is to attempt to develop structural failure limits for the Mission AS-204 launch vehicle when the effect of elevated temperatures on the structural capability is considered. Previous limits were derived from simulation cases where failures occurred early in flight and the effects of aerodynamic heating were assumed to be negligible (Reference 1).

The structural loads were derived from the TRW "N-Stage" digital program (Reference 1). Temperature histories of the vehicle components were computed for each of the trajectories using the TRW Ascent Heating Program (Reference 2). In the early work the complete temperature distribution for the components that make up the service module - spacecraft lunar module adapter (SM-SLA) interface and the SLA-IU interface were computed using the Ascent Heating Program and the TRW Thermal Analyzer Program (Reference 3). Further analysis showed that only the Ascent Heating Program was required after the critical components were identified. The areas of the spacecraft considered in this study are shown in Figure 1-1.

The effects of winds and wind shear on the thermo-structural limits were evaluated to determine the dependency of the limit lines on wind variations. The wind profiles used are shown in Figure 1-2.

The trajectories that were analyzed were limited to those cases where the malfunctions result in relatively slow changes in vehicle attitude and where the variations in the trajectory parameters are readily discernible from the "nominal trajectories." In all cases analyzed the malfunctions were limited to the gyro drift failure mode.

### 1.1.1 Ground Rules

The following assumptions were made for the thermo-structural limits portion of the task. These items are in addition to the assumptions

used in the trajectory development and the determination of interface loads.

1) The gyro drift malfunctions used to develop the limit lines were initiated at lift-off. Additional trajectories with gyro drift initiated late in flight were analyzed to determine the validity of the limit lines.

2) A single, high-density perturbation of the Patrick AFB reference atmosphere was used.

3) Only downrange dispersions were used in developing the thermo structural limits.

4) Wind profiles with the maximum shear occurring at any altitude other than approximately 10 km were not considered.

5) Structural strength of the SM-SLA interface was derived from room temperature test data. (See Discussion for methods used to extrapolate the data to higher temperatures.)

## 1.2 SUMMARY

The following conclusions summarize the results of this study.

1) The SM skin in the SM-SLA interface is the most critical component for the trajectories considered.

2) The SM skin temperature can be computed using adiabatic wall techniques (Eckert's method).

3) Use of trajectory parameters (AHI) to predict skin temperatures is not feasible due to limitations in determining angle of attack.

4) Use of a single AHI or skin temperature value could cause a 10 second error in the predicted time of failure versus the calculated failure time.

5) The use of an inertial velocity-flight path angle display to detect thermo-structural failures is not recommended when variations in gyro drift rate and failure time are considered.

6) The thermo-structural failure line on a relative velocity-altitude display provides a limit independent of atmospheric conditions when the prelaunch measured atmospheric conditions are used in the real-time display computations.

### 1.2.1 Restrictions on the Use of Limits

The limiting conditions defined in this report are subject to certain restrictions due to the assumptions made in the derivation and the limits imposed on the study. These restrictions are due to the following items:

1) Only a single mode of failure was considered (gyro drift).

2) The direction of gyro drift was limited to the pitch plane in the downrange direction.

3) The limit line is only applicable for a power-on launch vehicle in the lift-off configuration (prior to abort).

4) Flight in the region beyond the limit line should be treated as a high risk zone, but not necessarily as an absolute failure region, since conservatism has been used in the derivation of the thermo-structural limits.

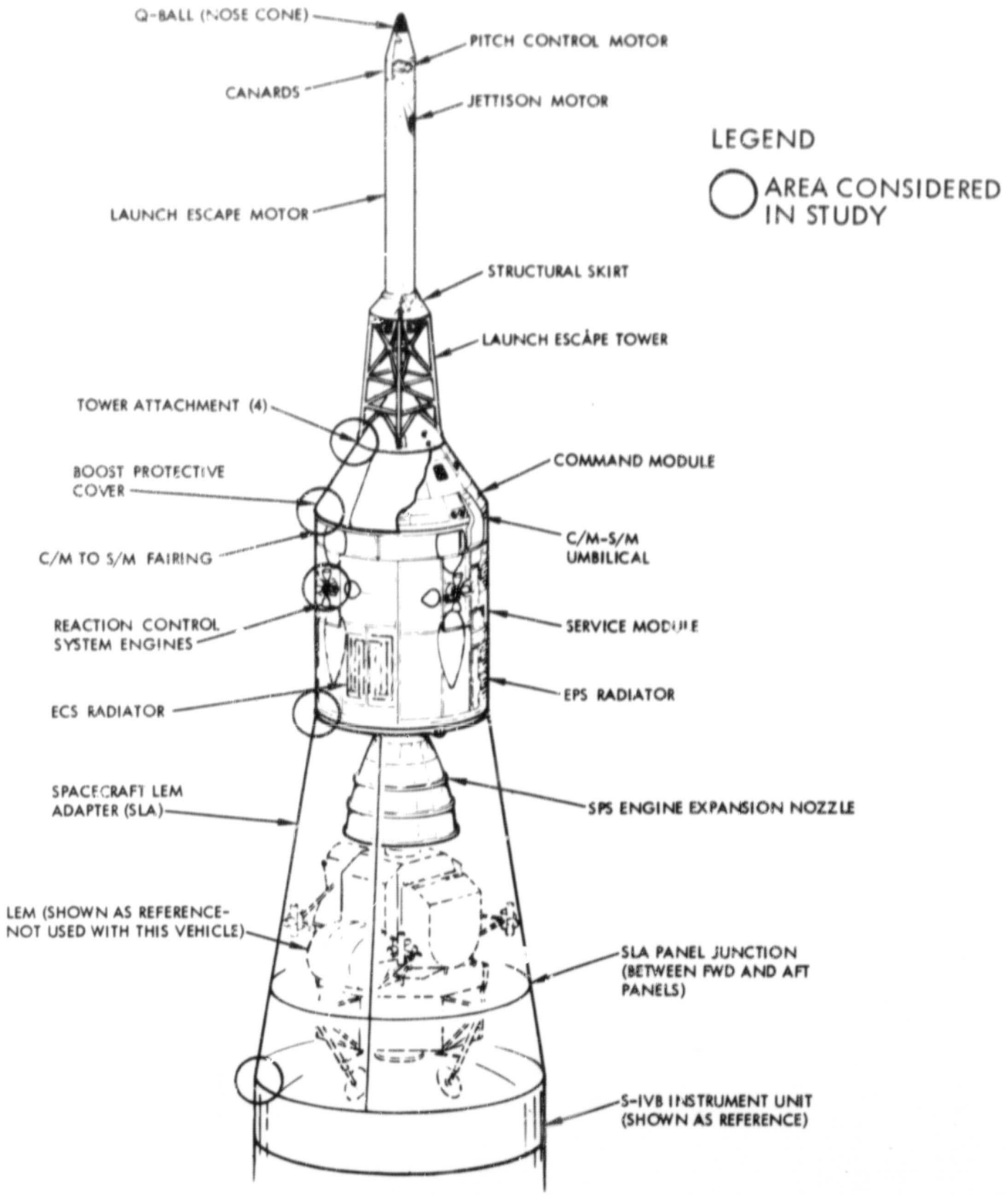


Figure 1-1. Launch Vehicle Geometry - Spacecraft Components

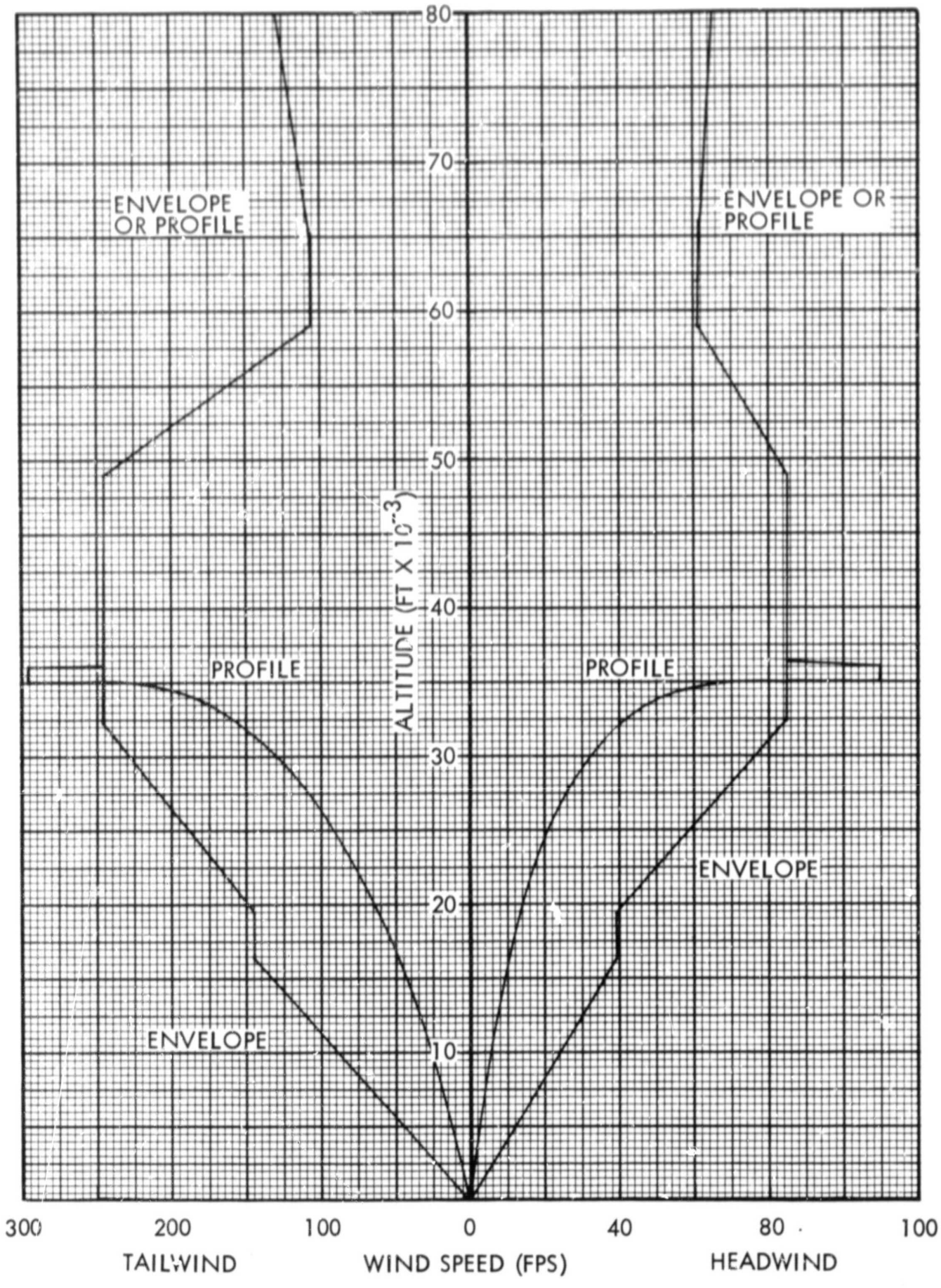


Figure 1-2. Synthetic Wind Profiles

# 2. DISCUSSION

The methods used to generate the thermo-structural limits are detailed below.

## 2.1 AERODYNAMIC HEATING

An ascent heating program was developed for use in determining the aerodynamic heating and skin temperatures. This computer program (Reference 2) was a modification of a program used by the NASA-MSFC for launch vehicle heating (Reference 4). The major modification to the program was the addition of an option to compute local flow properties based on pressure distributions obtained from wind tunnel tests and verified by flight test. This option allowed the computation of leeward side heating in addition to windward side heating. This capability was required since the trajectory dispersions were such that different sides of the vehicle were windward at various times in the trajectory (Figure 2-1). The equations and methods used in the derivation of local flow properties are contained in Reference 5. The local flow properties may be computed for the SM-SLA interface, for the SLA, for the SLA-IU interface, and for the SIVB.

The basic heating analysis incorporates the Eckert Flat Plate Techniques (Reference 6) for laminar flow solutions and the Van Driest Techniques (Reference 7) for turbulent flow solutions. A heat balance was performed for a typical model of the service module honeycomb panel and resulted in transient temperature profiles for the honeycomb face sheets. The heat balance included internal and external radiation, convection, conduction and heat stored terms.

The 3 sigma dispersed atmosphere which was used for the trajectory simulations has also been used for the determination of heating rates to insure compatibility of loads and skin temperatures.

## 2.2 STRUCTURAL METHODS

The structural analysis presented herein, extends the Reference 1 analyses to include the effects of aerodynamic heating on the vehicle. This heating results in a degradation of the vehicle structural capability

# 2. DISCUSSION

The methods used to generate the thermo-structural limits are detailed below.

## 2.1 AERODYNAMIC HEATING

An ascent heating program was developed for use in determining the aerodynamic heating and skin temperatures. This computer program (Reference 2) was a modification of a program used by the NASA-MSFC for launch vehicle heating (Reference 4). The major modification to the program was the addition of an option to compute local flow properties based on pressure distributions obtained from wind tunnel tests and verified by flight test. This option allowed the computation of leeward side heating in addition to windward side heating. This capability was required since the trajectory dispersions were such that different sides of the vehicle were windward at various times in the trajectory (Figure 2-1). The equations and methods used in the derivation of local flow properties are contained in Reference 5. The local flow properties may be computed for the SM-SLA interface, for the SLA, for the SLA-IU interface, and for the SIVB.

The basic heating analysis incorporates the Eckert Flat Plate Techniques (Reference 6) for laminar flow solutions and the Van Driest Techniques (Reference 7) for turbulent flow solutions. A heat balance was performed for a typical model of the service module honeycomb panel and resulted in transient temperature profiles for the honeycomb face sheets. The heat balance included internal and external radiation, convection, conduction and heat stored terms.

The 3 sigma dispersed atmosphere which was used for the trajectory simulations has also been used for the determination of heating rates to insure compatibility of loads and skin temperatures.

## 2.2 STRUCTURAL METHODS

The structural analysis presented herein, extends the Reference 1 analyses to include the effects of aerodynamic heating on the vehicle. This heating results in a degradation of the vehicle structural capability

and causes structural failures in addition to those included in the Reference 1 report.

The effects of aerodynamic heating on the launch escape system-command module (LES-CM) and command module-service module (CM-SM) interfaces were neglected due to thermal isolation and protection.

The structural capability of the SM-SLA interface at room temperature was based on the static structural tests presented in Reference 8. It was assumed that the test loads represent the ultimate room temperature structural capability of the interface at the maximum dynamic pressure-angle of attack combination ($q\alpha$). The ultimate maximum $q\alpha$ axial load and bending moment were used to calculate an equivalent axial load capability of 570,000 lbs. at room temperature. It should be noted that during the first stage end boost test condition (Saturn V loads), the SM aft bulkhead prematurely failed at 140% limit load instead of the required 150% limit load. The failure equivalent axial load was calculated to be 513,000 lbs. Since, this failure was not due to body loads, but due to a localized effect, and the basic structural shell did not fail; it was assumed that the maximum $q\alpha$ equivalent axial load was the room temperature structural capability of the SM-SLA interface (Reference 9).

The structural capability of the interface at elevated temperatures was assumed to be dependent upon the SM outer skin. This assumption was based on a two-dimensional thermal model, which calculated the temperature history distribution throughout the interface. It was found that the SM outer skin was at the highest temperature and its structural properties were most severely degraded by temperature. This fact is illustrated in the following figure. The figure presents the thermo-structural capability of two components in the SM-SLA interface versus the time of flight for a typical trajectory.

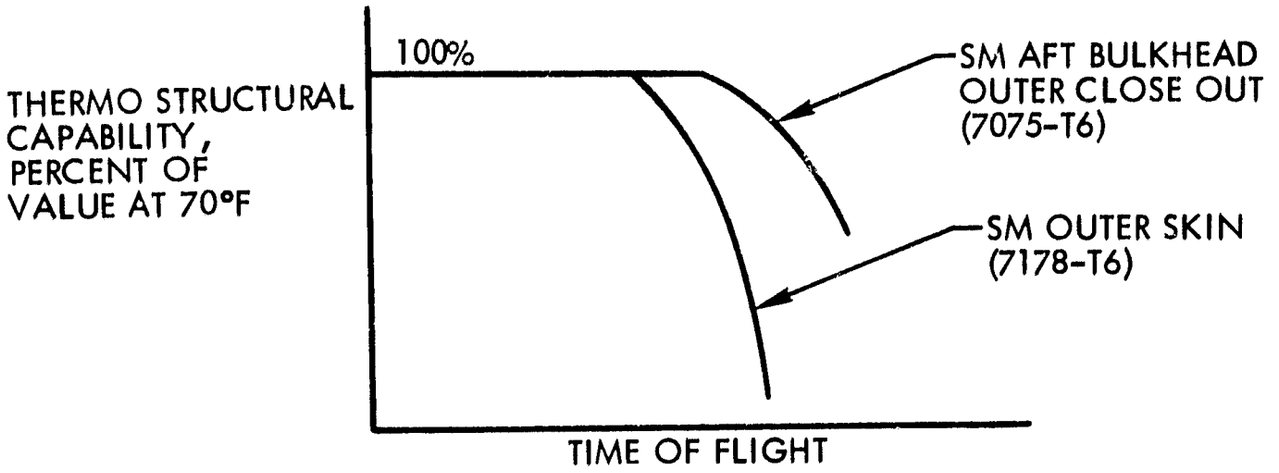


Thus it can be seen that the thermo-structural capability of the SM outer skin degrades much faster than the SM aft bulkhead outer closeout. This relationship is also applicable for all interface components.

It was assumed that the SM-SLA interface structural capability was degraded in the same manner by temperature as the compressive yield strength of the 7178-T6 aluminum alloy face sheet. Reference 10 was used to obtain the temperature degradation curve for the material. This degradation curve is based on half (1/2) hour exposure times and the actual mission exposure times are much shorter. This will introduce a conservative factor into the capability, since the half hour properties reduce the equivalent axial load capability at elevated temperatures more than the short time exposure properties. Figure 2-2 shows the SM-SLA interface structural capability at elevated temperature used for this study. The thermo-structural zero load capability cut off point at T = 550° F was obtained from MSC/SMD personnel. It is based on deterioration of the face sheet bond with temperature.

With the SM-SLA interface thermo-structural capability defined, the selected trajectories were analyzed for structural failures that occurred

during the first stage boost. For each trajectory under analysis, the loads at selected body stations were calculated by use of the Reference 1 computer program. The program calculated the rigid body loads at each body station. To account for flexible body effects, dynamic load factors were applied to the rigid body loads. These dynamic load factors were obtained from MSFC and MSC personnel (Reference 1). The factors were conservatively high and yielded conservative structural loads. A more detailed explanation of these calculations is contained in Reference 1. The loads were then correlated with the temperatures calculated by the Reference 2 computer program. These loads and temperatures were then plotted against the interface thermo-structural capability. A failure was determined when the two curves crossed. Figures 2-3, 2-4, and 2-5 present three typical trajectories that were analyzed. As can be seen in Figures 2-3 and 2-5, the exact point of failure is difficult to determine because of the erratic behavior of the loads. A finer time step in the computer program would facilitate a more accurate solution. Figure 2-4 shows a typical "no failure" case.

The SLA-IU interface structural capability at elevated temperatures was determined from Reference 11 in the same manner as for the SM-SLA. interface. Analysis of this interface indicated that it was less critical than the SM-SLA interface. This was attributed to several things. The temperatures were considerably lower, while the load-capability relationship was approximately the same. Thus, for those trajectories analyzed no failures were indicated.

## 2.3 AERODYNAMIC HEATING INDICATOR

An attempt was made to correlate a combination of trajectory parameters with the skin temperature of the SM-SLA interface. This was done with an aerodynamic heating indicator (AHI) of the following form:

$$AHI = \int \rho_\infty V_{REL}^3 dt,$$

where,

$\rho_\infty$ = free stream density, and

$V_{REL}$ = velocity of the vehicle with respect to the wind.

Figure 2-6 shows that the effect of wind on the correlation is large and precludes the use of this form of AHI. The major cause of the disagreement is the change in local flow properties, and therefore local heating, due to differences in the angle of attack. It is possible that some form of the AHI where the angle of attack is included could provide closer correlation. However, the inflight angle of attack is difficult to obtain and the accuracy of angles derived from trajectory parameters or the "Q-ball" would have to be investigated in more detail.

## 2.4 TWO DIMENSION THERMAL MODELS

Thermal models of the SM-SLA and SLA-IU interfaces were developed using a two dimensional radiation - conduction network in conjunction with the TRW Thermal Analyzer Program (TAP). Nodal locations for the two interfaces were established on certain interface components to determine the temperature distribution throughout the structure. Geometry and nodal networks for the two interfaces are shown in Figures 2-7 through 2-11. A total of 24 nodes were used for the SM-SLA interface.

Aerodynamic heating rates were determined for several values of constant wall temperature using the Ascent Heating Program. The heating rates were input to the TAP program and interpolated based on the TAP computations of wall temperature.

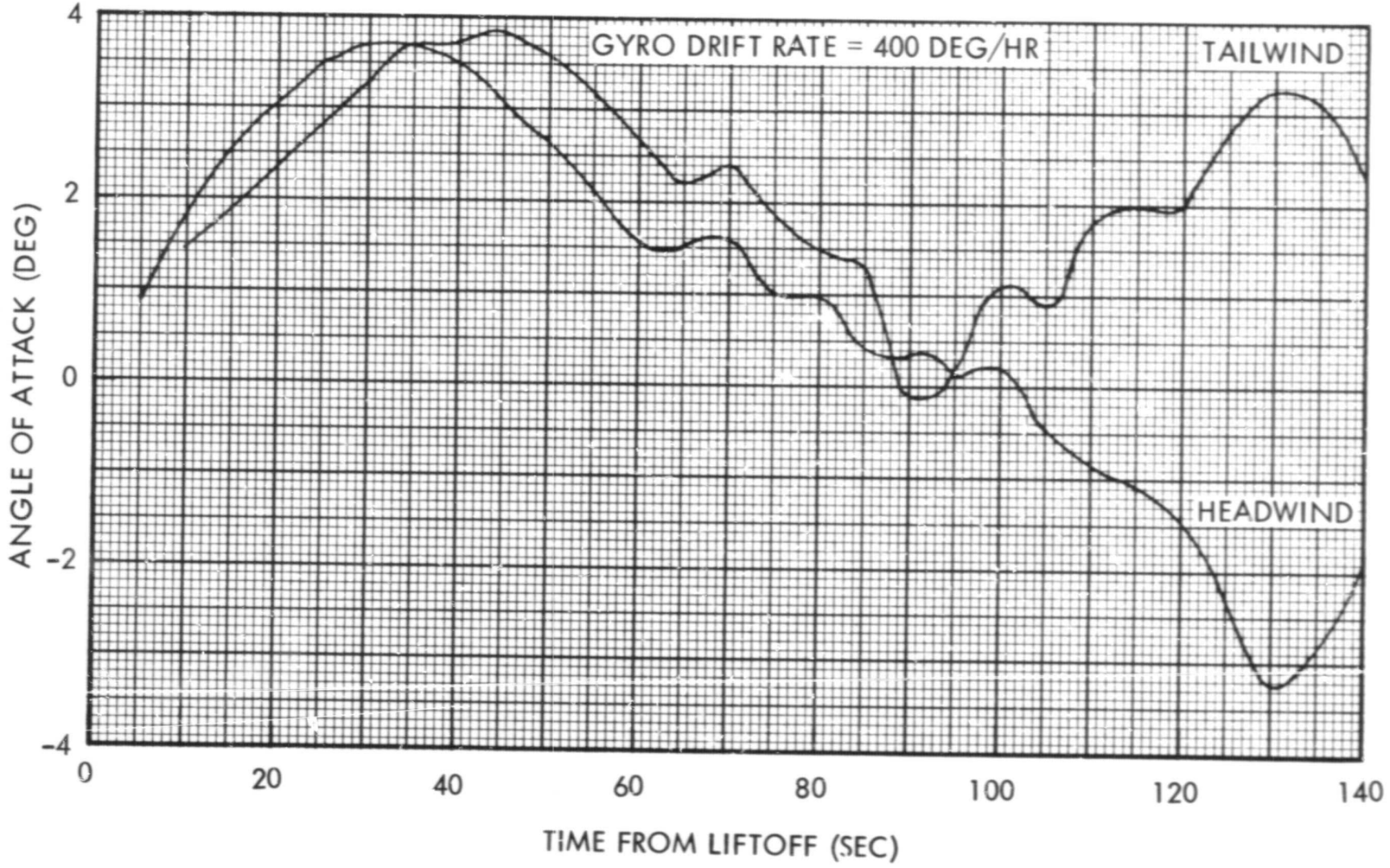


Figure 2-1. Typical Angle of Attach Histories

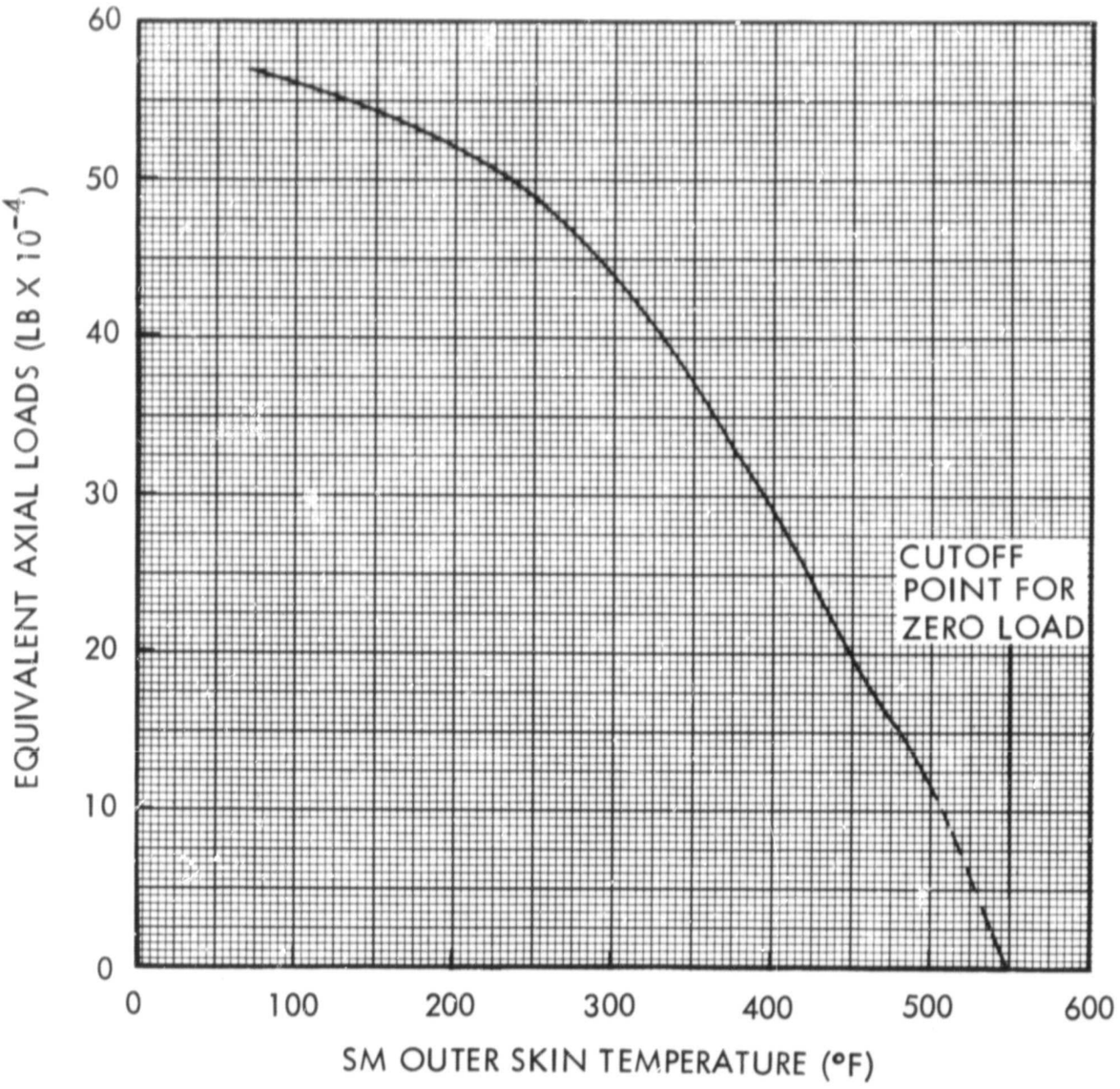


Figure 2-2. SM Outer Skin Structural Capability at Elevated Temperatures

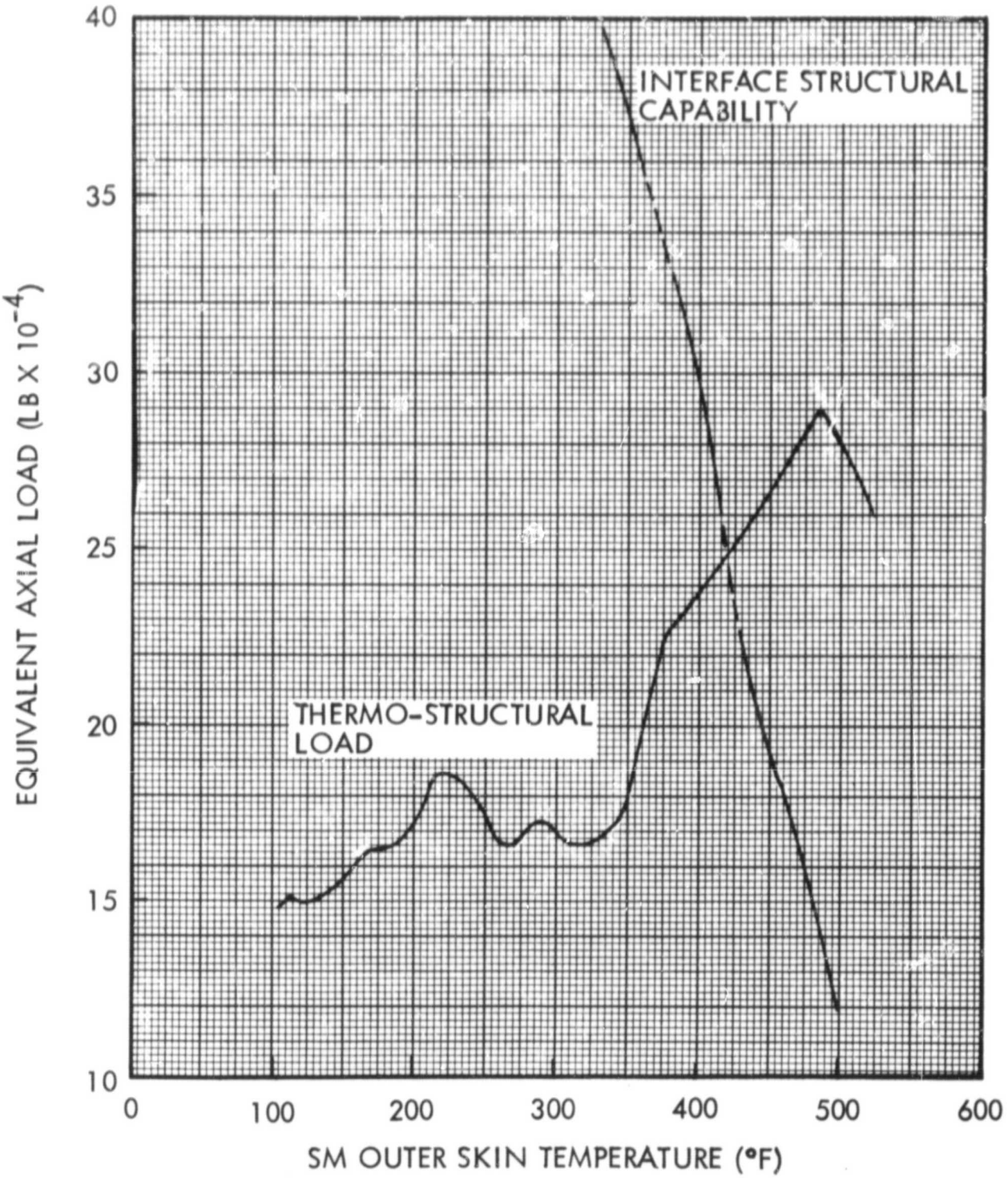


Figure 2-3. Typical Thermo-Structural Failure - SM-SLA Interface

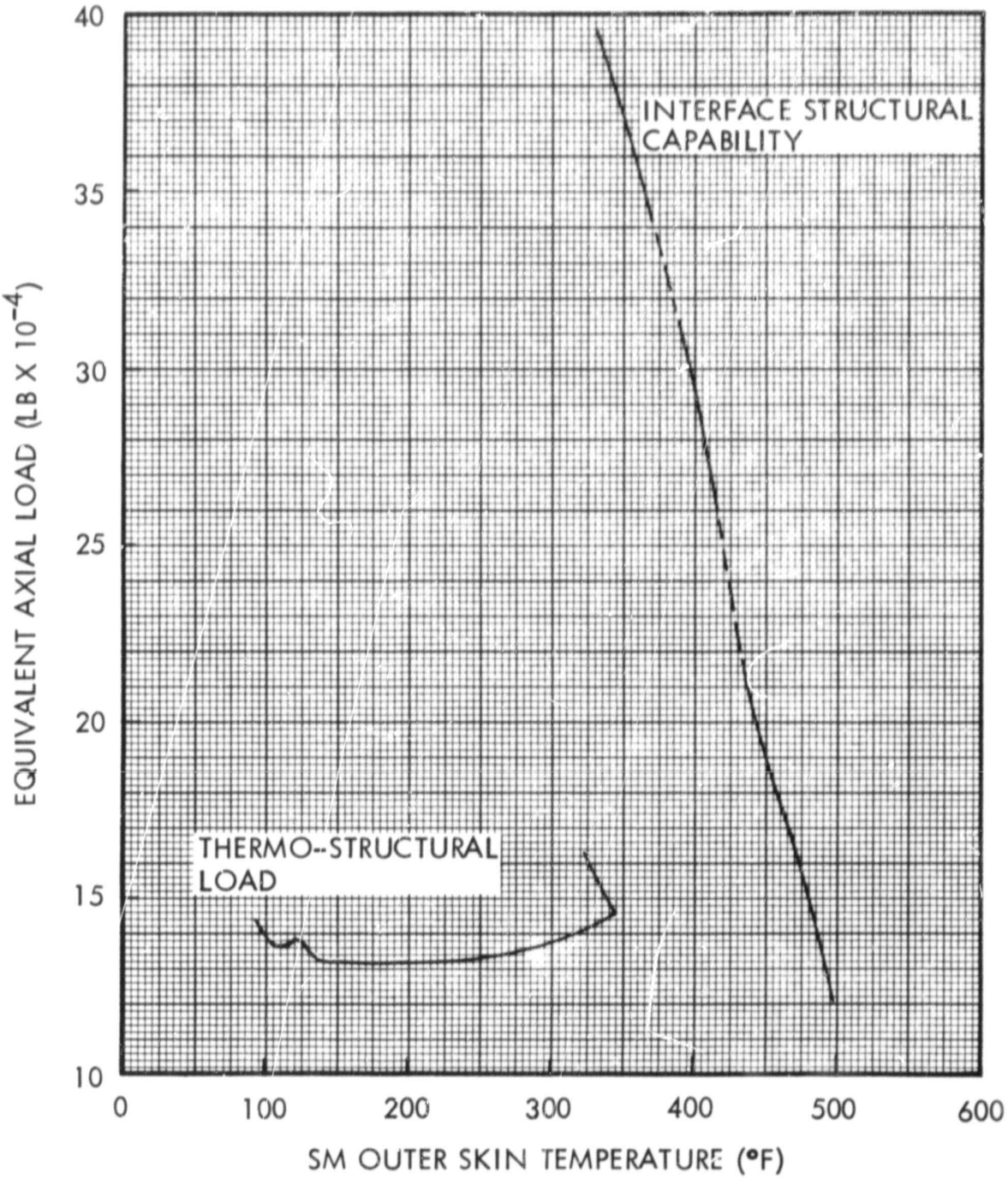


Figure 2-4. Typical "No Failure" Case - SM-SLA Interface

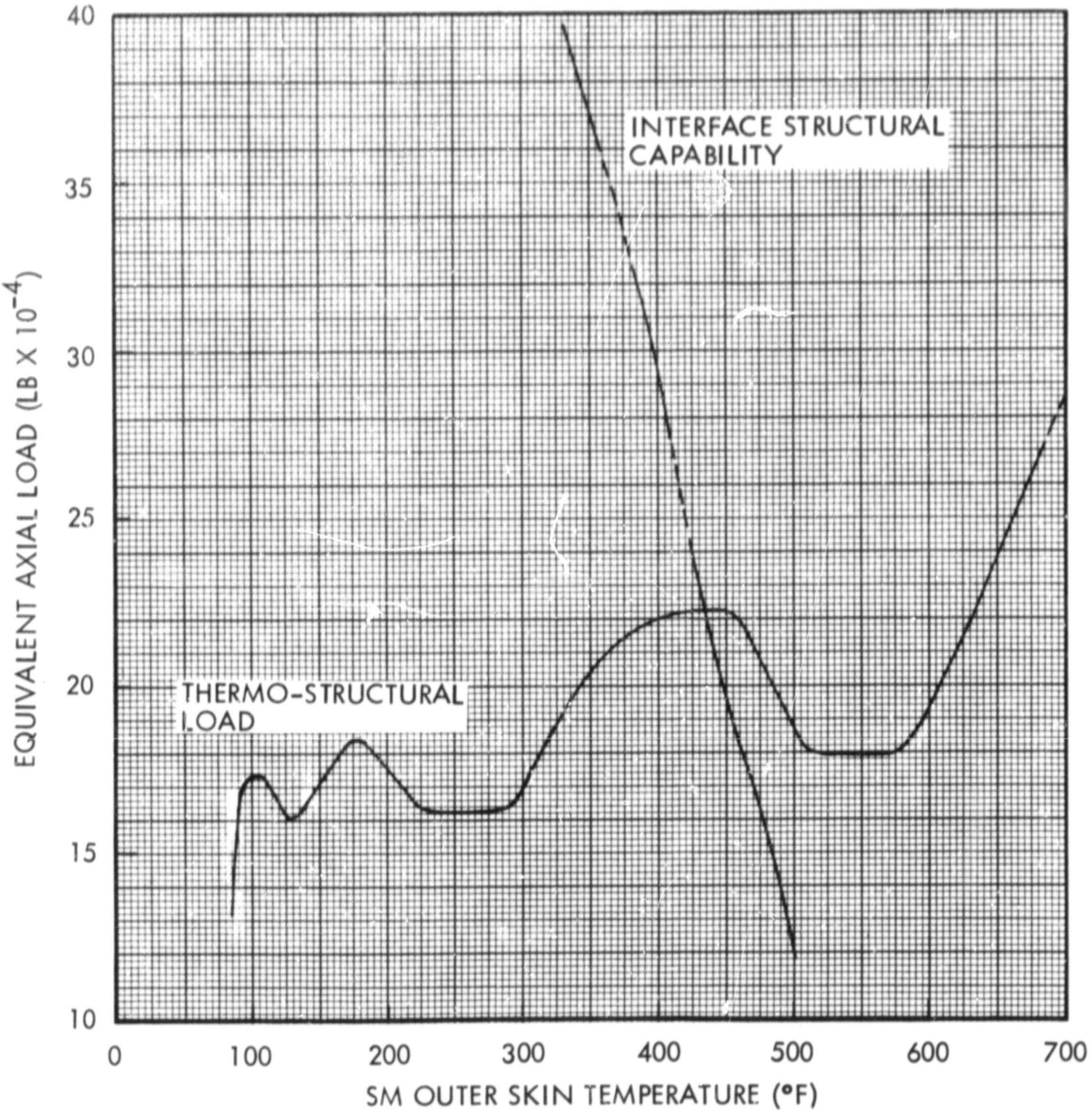


Figure 2-5. Typical Thermo-Structural Failure - SM-SLA Interface

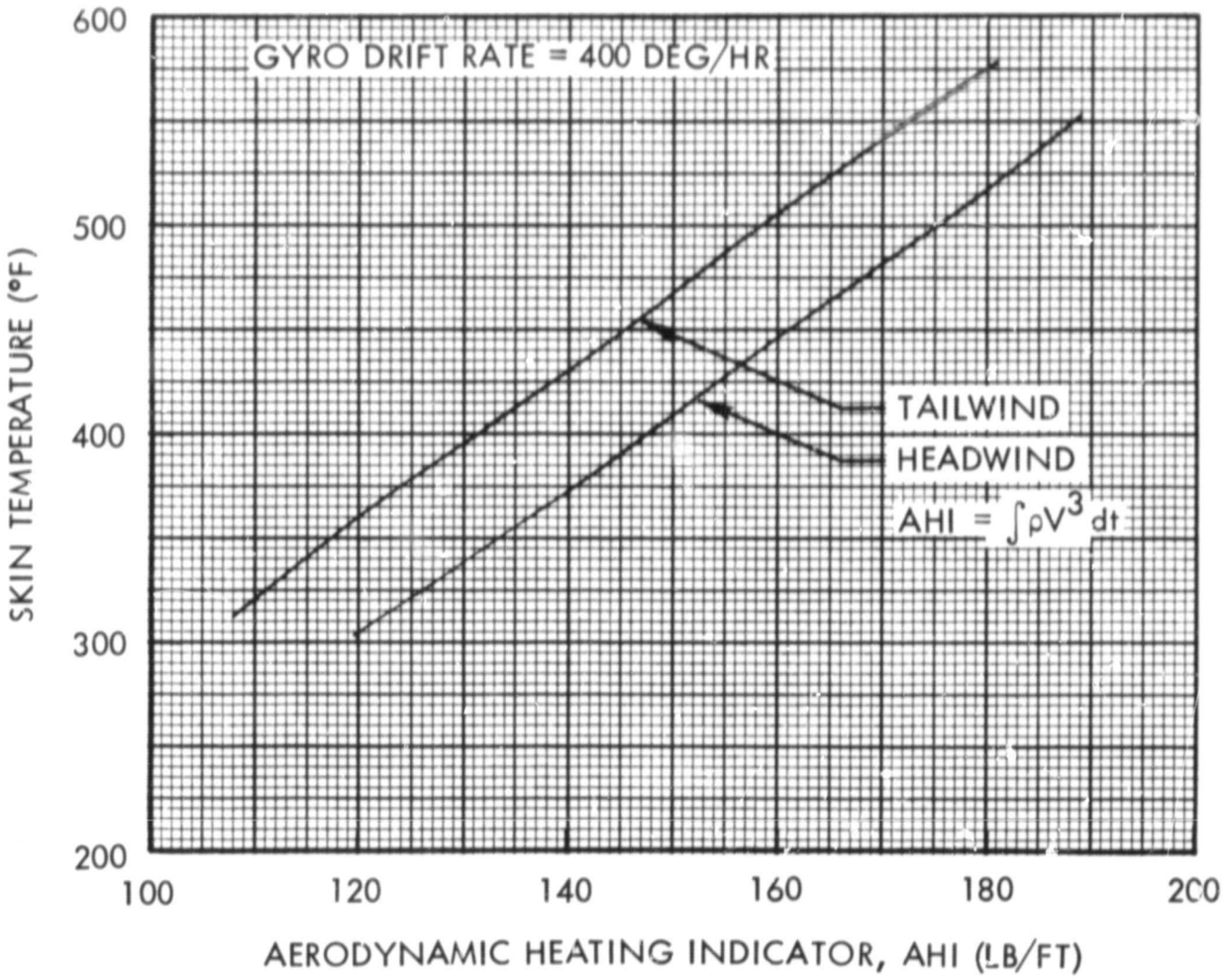


Figure 2-6. SM Skin Temperature - AHI Correlation

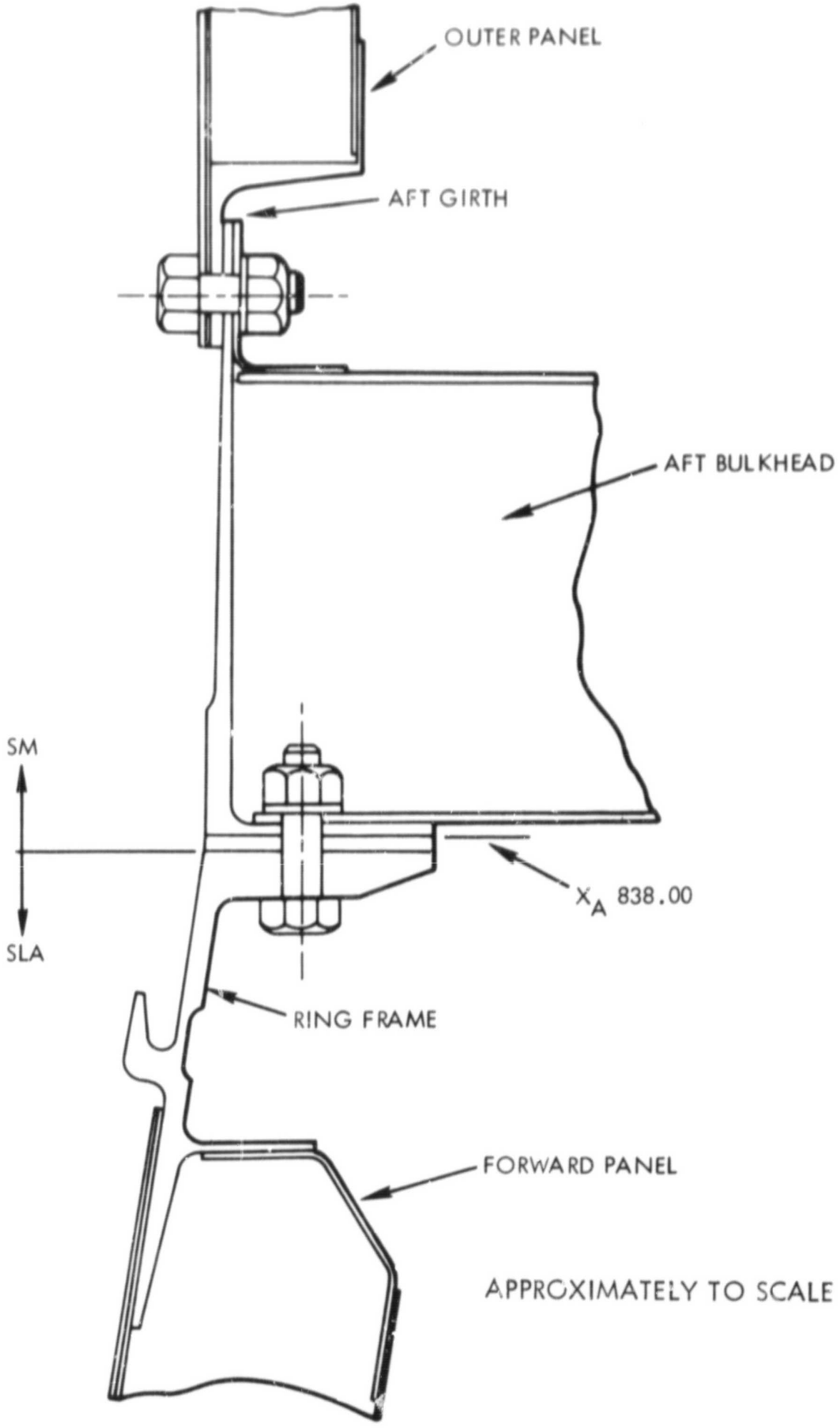


Figure 2-7. AM-SLA interface Geometry

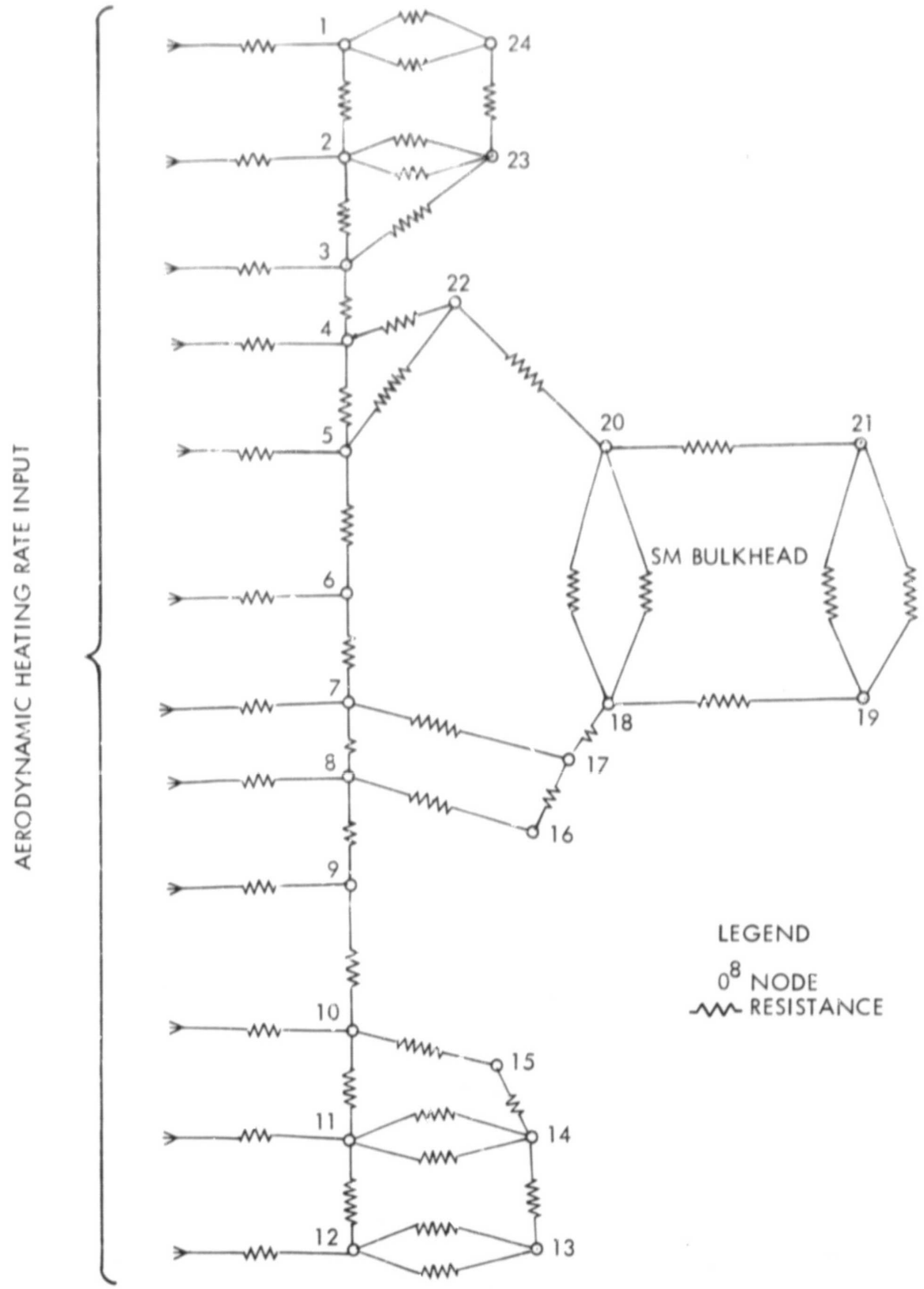


Figure 2-8. SM-SLA Interface Thermal Network

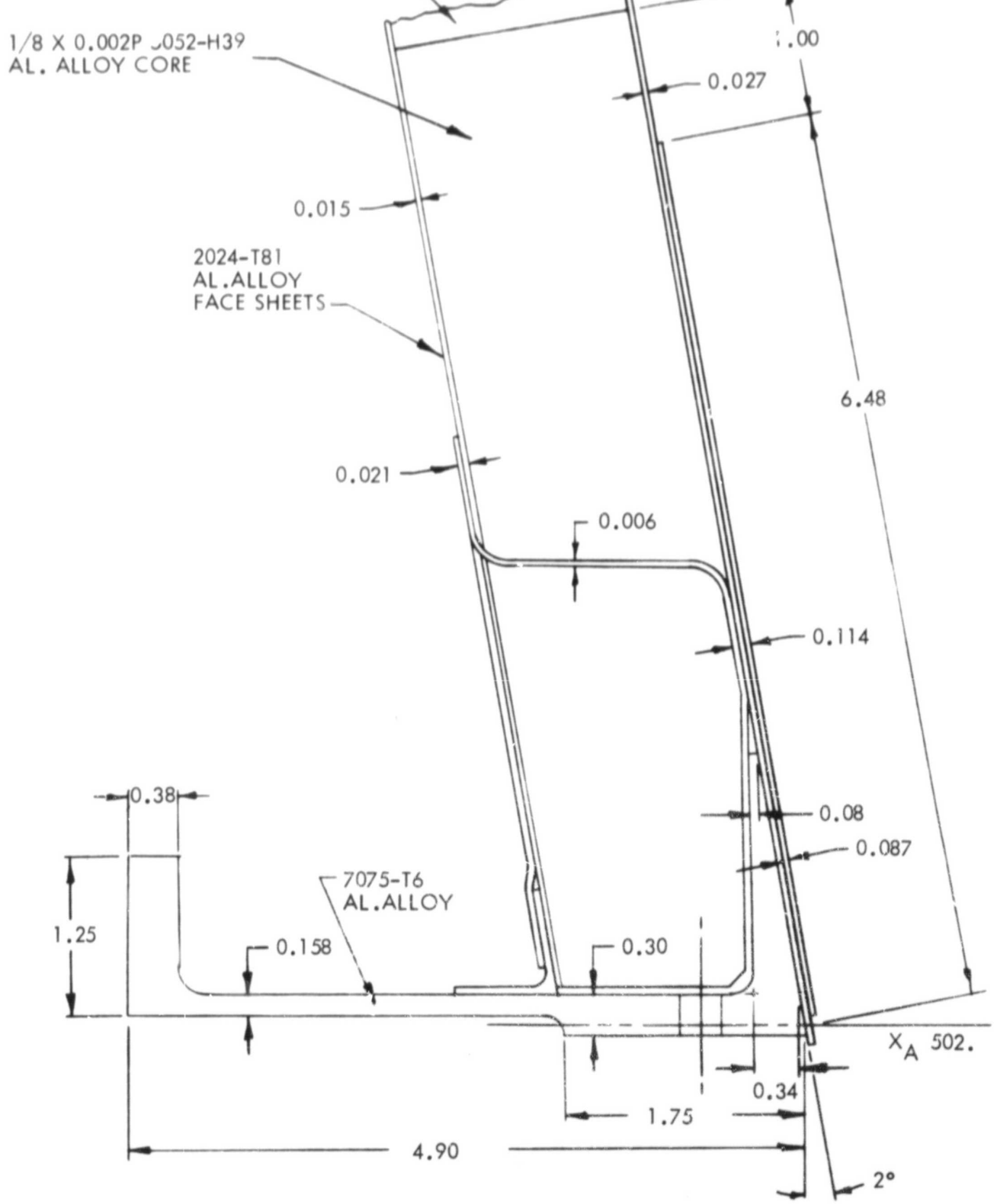


Figure 2-9. SLA-IU Interface Geometry - SLA

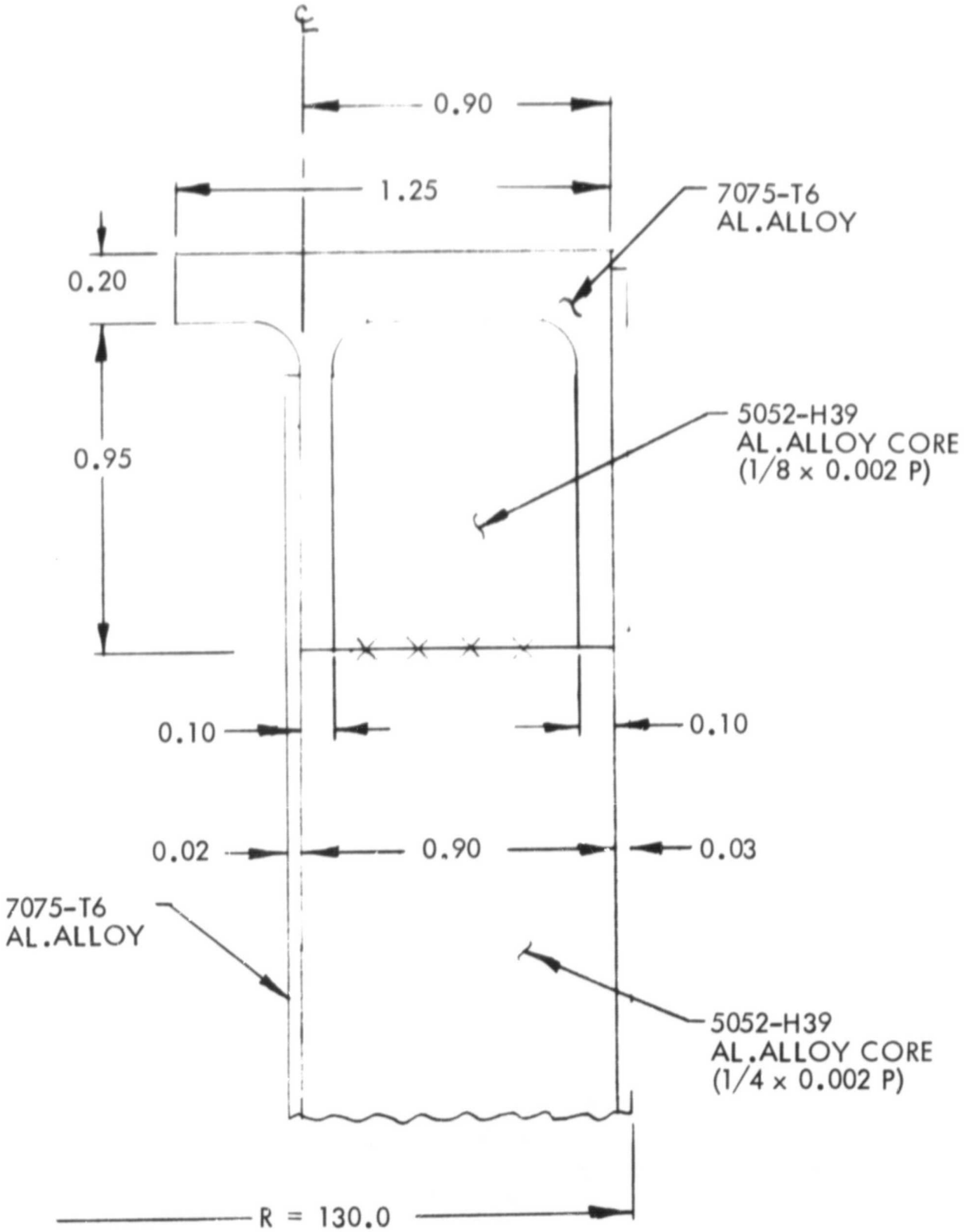


Figure 2-10. SLA-IU Interface Geometry

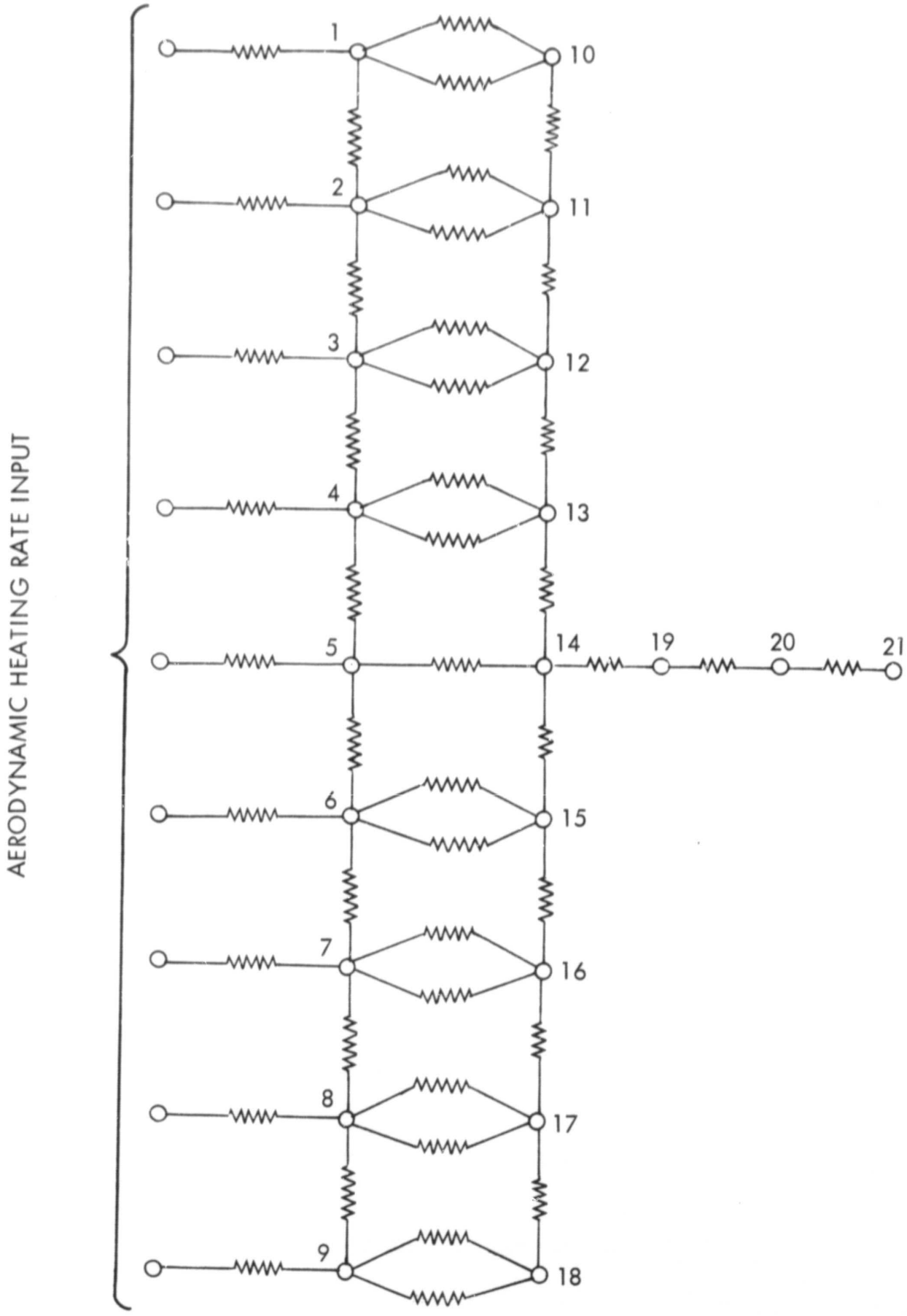


Figure 2-11. SLA-IU Interface Thermal Network

# 3. RESULTS

The results of the thermo-structural analyses are summarized in Table 3-1 which includes a description of the cases analyzed and the conditions at failure, where applicable. The failure limits determined by this study were derived by considering only a single type of launch vehicle malfunction and are subject to the limitations imposed by the assumptions and ground rules.

## 3.1 CRITICAL AREAS

Early in the study it was determined that the critical interface was the SM-SLA interface and the SM skin immediately forward of SM bulkhead was the critical component due to its sensitivity to aerodynamic heating. This is logical since the SM outer face sheet is the thinnest skin in the SM-SLA interface, and the aerodynamic heating is approximately equal throughout the area. The CM-LES interface was not considered since it is protected during launch by the boost protective cover "cuffs." Although the room temperature structural capability of the SLA-IU is approximately the same as the SM-SLA interface, the temperatures in that region are considerably cooler. The maximum temperature in the SLA-IU region was approximately 300°F, whereas the SM skin was failing at approximately 470°F for the trajectories considered. The CM-SM interface was not considered due to the protection afforded by the SM fairing.

The SM-RCS quad was eliminated from consideration as a critical component by reviewing the methods used for the design analysis (Reference 12). The analysis was highly conservative and the design trajectories were similar to those during which SM skin failure occurred in this study. The skin adjacent to the quads was eliminated as a critical candidate by using a highly conservative analysis of the heating in this area and considering the large heat sinks available. Thus, the limit lines contained in this report are based only on the SM skin temperatures.

Although the two-dimensional thermal models were used in the early part of the study, it was determined that an option of the Ascent Heating Program to compute the temperature of a honeycomb panel was more than adequate and was used in the final determination of SM skin temperatures

for the structural analysis. The temperature distribution of the outer skin of the SM-SLA interface for a typical condition is shown in Figure 3-1.

## 3.2 THERMO-STRUCTURAL LIMITS

The thermo-structural limits for the gyro drift failure modes may be displayed in a variety of ways. Analysis has shown that it is not possible to isolate the structural failure into an independent structural loading condition or to a single value of skin temperature. Attempts were made to utilize various displays to depict the limits. The most promising of these are the inertial velocity-flight path angle, and the altitude-relative velocity displays.

### 3.2.1 Inertial Velocity-Flight Path Angle Display

The thermo-structural limits are shown on a display of inertial velocity - inertial flight path angle display in Figure 3-2. The limits are shown for the no wind, head wind, and tailwind conditions. Variations of the trajectories and the limits due to use of the wind envelopes or the wind profiles in a specific direction were negligible except for one case in which rapid divergence of the launch vehicle occurred at 94 seconds when the head wind profile was used with the 660 degree per hour drift rate trajectory. Structural failure for the same drift rate with the head wind envelope occurred at 112 seconds due to thermo-structural failure. Similar cases probably exist when wind profiles with high values of wind shear are combined with high drift rates. This type of failure should probably be classified as a rapid divergence failure and must be detected by methods other than the thermo-structural limits on a trajectory parameter display.

Three trajectory cases (124, 125, and 126) were used to determine the validity of the limit on the velocity-flight path angle display. These trajectories were developed by using a zero gyro drift rate from lift-off to 80 seconds and then introducing a high drift rate throughout the remainder of the first stage boost. The rates were 900, 1100, and 1300 degrees per hour for cases 124, 125, and 126, respectively. The velocity-flight path angle histories for these trajectories are shown on Figure 3-2. Cases 125 and 126 (1100 and 1300 deg/hr) penetrated the limit on this display at 133.8 and 130 seconds, respectively. However, examination of the

structural loads and skin temperatures shows that neither of these cases would fail. The load-temperature relationships for the three check cases are shown in Figure 3-3. The inertial velocity-flight path angle display is therefore not recommended for use in determining thermo-structural failures.

### 3.2.2 Relative Velocity-Altitude Display

The effect of winds on the thermo-structural limit line display can be eliminated if a relative velocity-altitude display is used. This display could be derived from tracking data and atmospheric properties measured prior to launch. The thermo-structural failure limits are shown in Figure 3-4 for cases including those with winds.

The three check cases are also shown in Figure 3-4. None of the three cases violated the thermo-structural line on this display, although Case 126 approaches the limit at 140 seconds after lift-off. This case would probably cross the limit if the analysis was continued beyond 140 seconds. This phenomenon can also be seen in the load-temperature relationship (Figure 3-3).

### 3.2.3 Other Displays

Attempts were made to correlate SM skin temperatures with the time of failure, but this system was not feasible since selection of a single value of skin temperature would cause an approximate error of 10 seconds in the prediction of failure. Use of a single value of the AHI also will cause a 10-second error in predicting the failure.

Table 3-1. Summary of Results

| Trajectory Number | Drift Rate (deg/hr) | Wind Direction | Type[1] | Thermostructural Failure | | | | |
|---|---|---|---|---|---|---|---|---|
| | | | | Time (sec) | Velocity (fps)[2] | Flight Path Angle (deg)[2] | Temperature (deg F) | Aerodynamic Heating Indicator (lb/ft x $10^{-6}$)[3] |
| 92 | 600 | None | | 116 | 5150 | 13.8 | 455 | 193.3 |
| 101 | 720 | None | | 110 | 4710 | 13.0 | 420 | 190.5 |
| 108 | 400 | None | | 126 | 5935 | 16.0 | 472 | 180.6 |
| 109 | 500 | None | | 121 | 5920 | 13.4 | 468 | 188.6 |
| 111 | 200 | TW | E | | No Failure | | | |
| 112 | 0 | HW | E | | No Failure | | | |
| 113 | 200 | HW | E | | No Failure | | | |
| 114 | 200 | None | | | No Failure | | | |
| 114A | 300 | None | | 134 | 6680 | 16.3 | 470 | 173.7 |
| 115 | 400 | HW | E | 125 | 5805 | 16.4 | 474 | 187.3 |
| 116 | 660 | HW | E | 112 | 4820 | 13.7 | 435 | |
| 117 | 400 | HW | P | 125 | 5805 | 16.4 | 473 | 198.9 |
| 118 | 660 | HW | P | 94 | 3600 | 19.7 | 222 | |
| 119 | 400 | TW | E | 127 | 6115 | 15.4 | 470 | 170.3 |
| 120 | 660 | TW | E | 113 | 5000 | 12.9 | 431 | 177.6 |
| 121 | 400 | TW | P | 128 | 6185 | 15.1 | 470 | 169.2 |
| 122 | 660 | TW | P | 114 | 5055 | 13.3 | 433 | 179.1 |
| 124 | (4) | None | | | No Failure | | | |
| 125 | (5) | None | | | No Failure | | | |
| 126 | (6) | None | | | No Failure | | | |
| 168 | 200 | Crosswind | E | | No Failure | | | |

[1] E = Envelope used as wind profile; P = Profile constructed with maximum shear at 10 km.

[2] Velocity and flight path angle for inertial reference system.

[3] $AHI = \int \rho_\infty V^3_{REL} dt$.

[4] $0 \leq$ Time $\leq 80$ sec, 0 deg/hr; 80 < Time $\leq 140$ sec, 900 deg/hr.

[5] $0 \leq$ Time $\leq 80$ sec, 0 deg/hr; 80 < Time $\leq 140$ sec, 1100 deg/hr.

[6] $0 \leq$ Time $\leq 80$ sec, 0 deg/hr; 80 < Time $\leq 140$ sec, 1300 deg/hr.

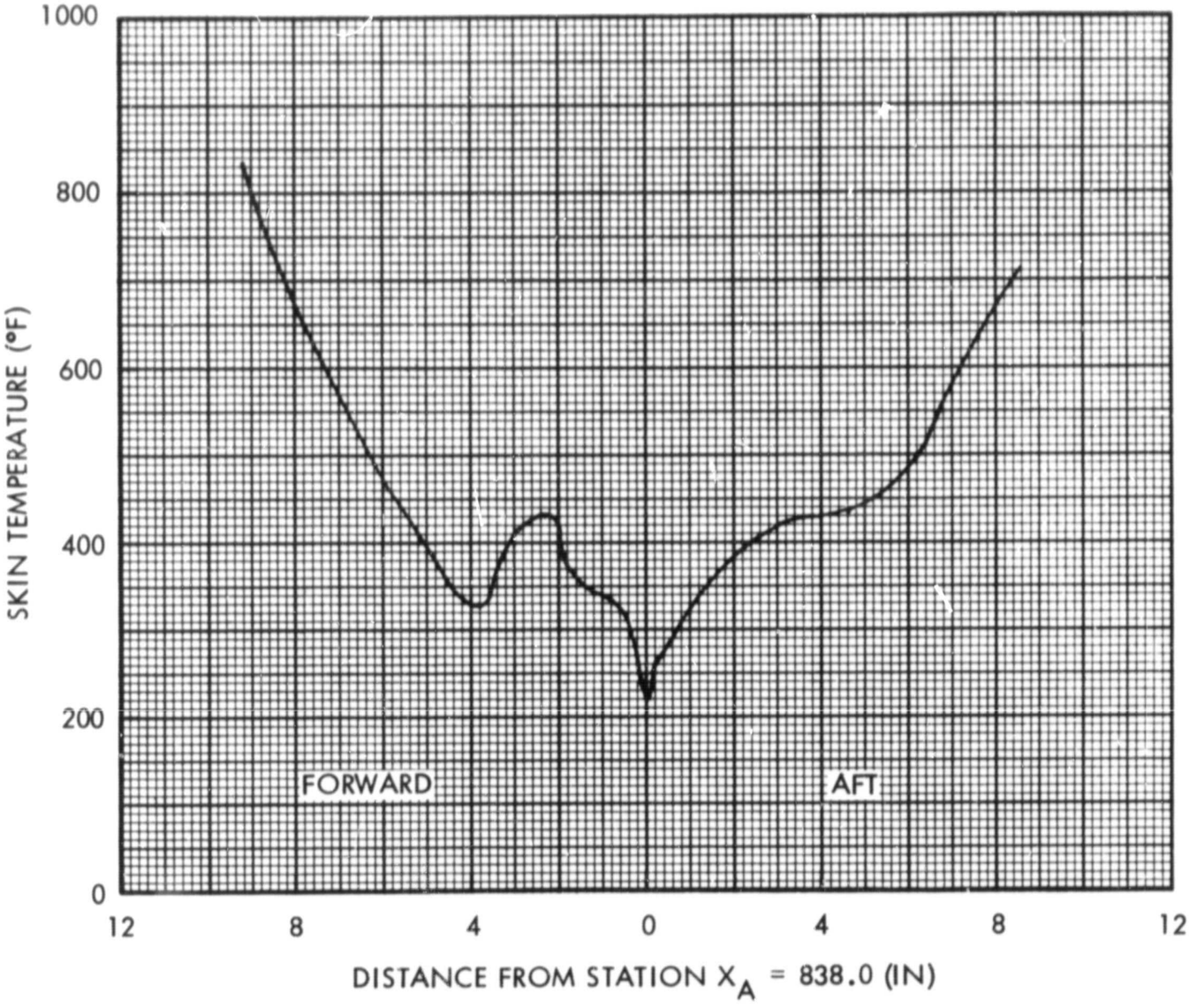


Figure 3-1. Temperature Distribution - SM-SLA Interface - Typical

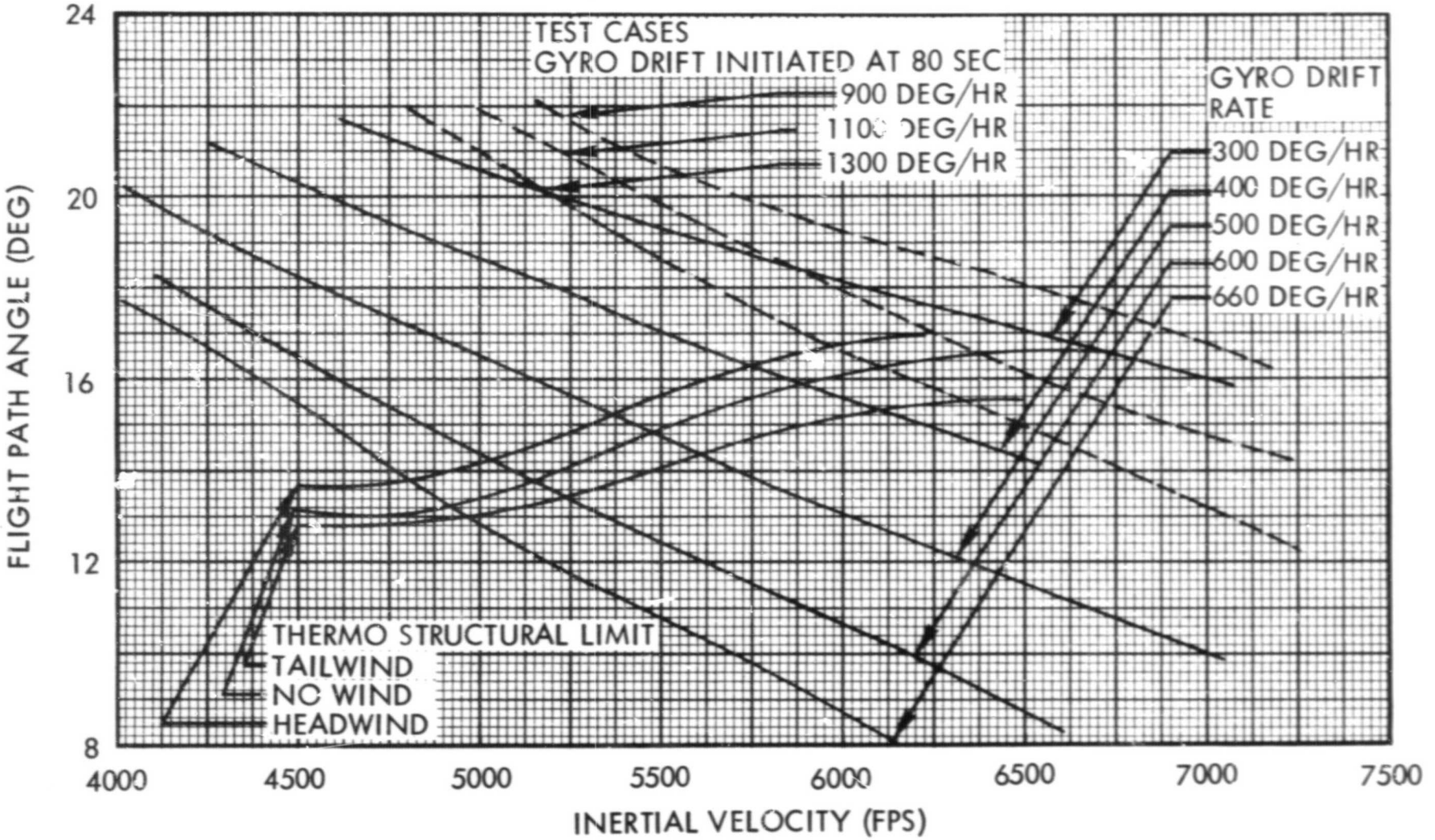


Figure 3-2. Thermo-Structural Limits - Inertial Velocity-Flight Path Angle Display

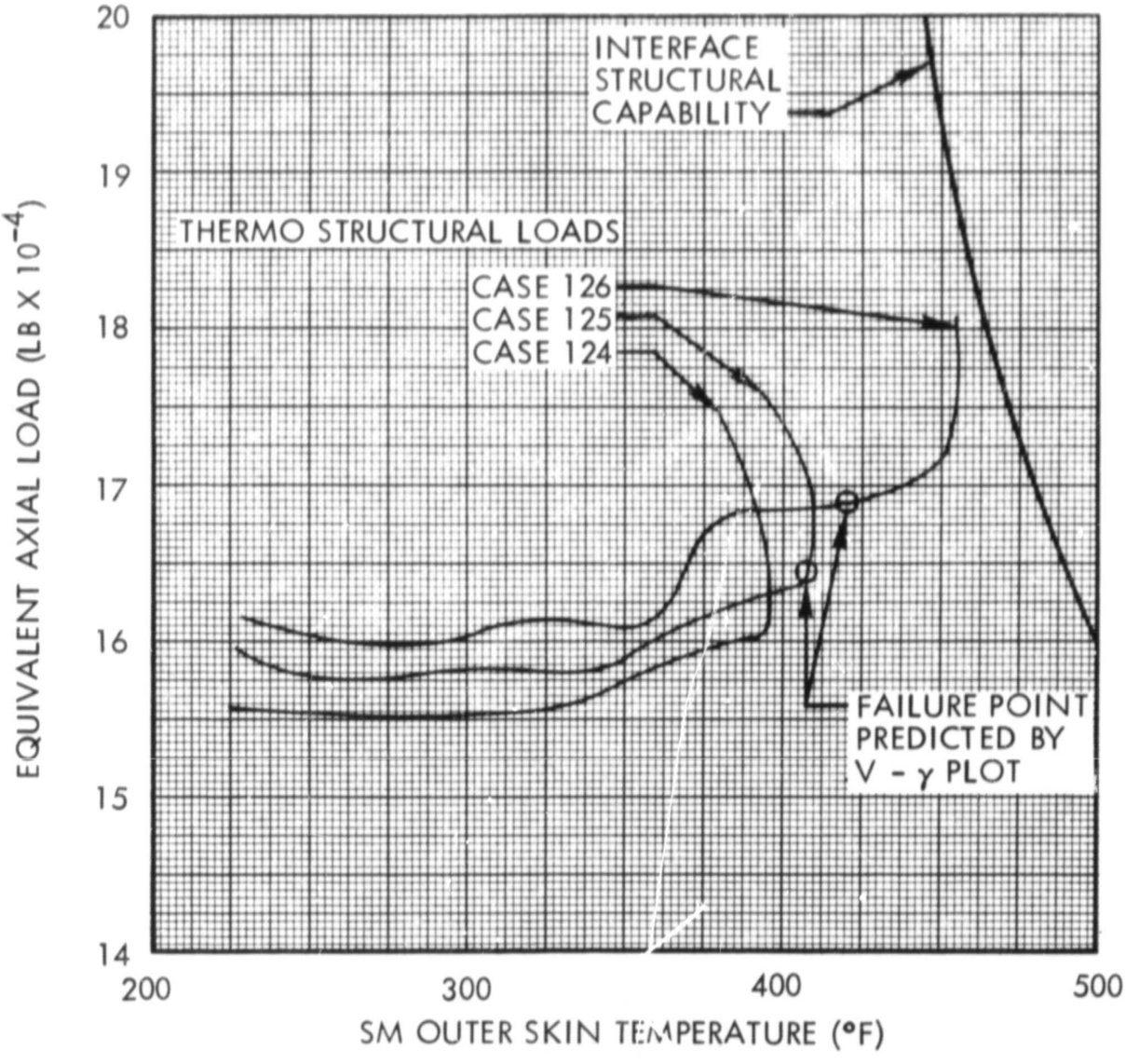


Figure 3-3. Thermo-Structural Loads - SM-SLA Interface - Delayed Gyro Drift Failure Mode

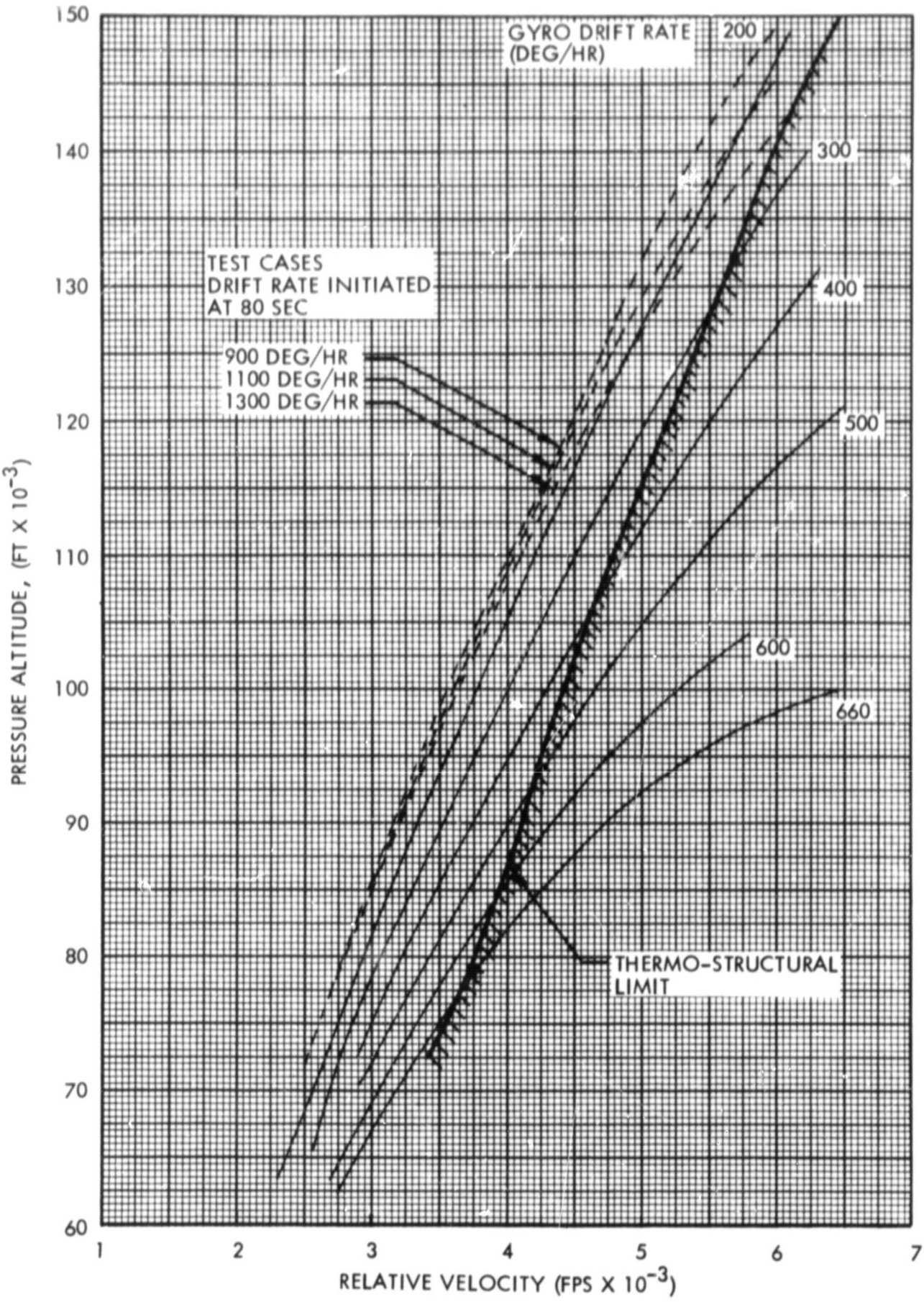


Figure 3-4. Thermo-Structural Limit - Altitude-Relative Velocity Display

# 4. RECOMMENDATIONS

The thermo-structural limit determined by this study should not be used for any abort initiation cue until the possibility of more restrictive limits detailed below is investigated further. Use of the limits, within the constraints of Section 1.2.1 for determining the region where a structural failure has a high probability of occurrence is valid.

It is recommended that the study be continued, since the feasibility of detecting structural failures at elevated temperatures has been demonstrated by this study.

## 4.1 MORE RESTRICTIVE LIMITS

For the flight regime considered in this study, it is possible that other limitations exist that are beyond the scope of this study. Such limits could invalidate portions of the study especially in those cases where no failures are indicated, such as gyro drift rates less than 300 degrees per hour. Limitations which should be examined before the thermo-structural limits are considered valid are as follows:

1) Thermo-structural limits for other failure modes should be determined.

2) End-boost transient loadings should be studied to insure that those cases in which no inflight thermo-structural failure is indicated will survive the end boost loads when the elevated temperatures are considered.

3) The region just prior to the thermo-structural limits should be investigated to determine the capability of the vehicle to survive the loadings due to abort and the engine shutdown. During the abort sequence additional loads are imposed due to the dynamics of the vehicle and the asymmetrical thrust which results from variations in the shutdown rates of the various engines.

4) The minimum altitude for the start sequence of the J-2 engine should be determined to insure those failure cases where no structural limits are violated will be able to go through a coast period and reach the minimum altitude at the proper time.

An attempt was made to determine the limiting conditions from which the launch could be completed to place the spacecraft in a nominal orbit. Figure 4-1 shows the first stage inertial velocity-flight path angle relationship for (1) a dispersion of the nominal trajectory where use of all the propellants (including reserves) was required to reach the orbit, and (2) a dispersion of the nominal trajectory where the vehicle tumbled during staging due to the loss of control. Also shown in Figure 4-1 is the thermo-structural failure line for zero winds. A comparison between the two limiting conditions shows that the thermo-structural limit is in a flight regime where the mission would probably be terminated due to the inability to reach a nominal orbit. The thermo-structural line does indicate that the flight cannot be continued and that a Mode I abort would be required prior to reaching this limit.

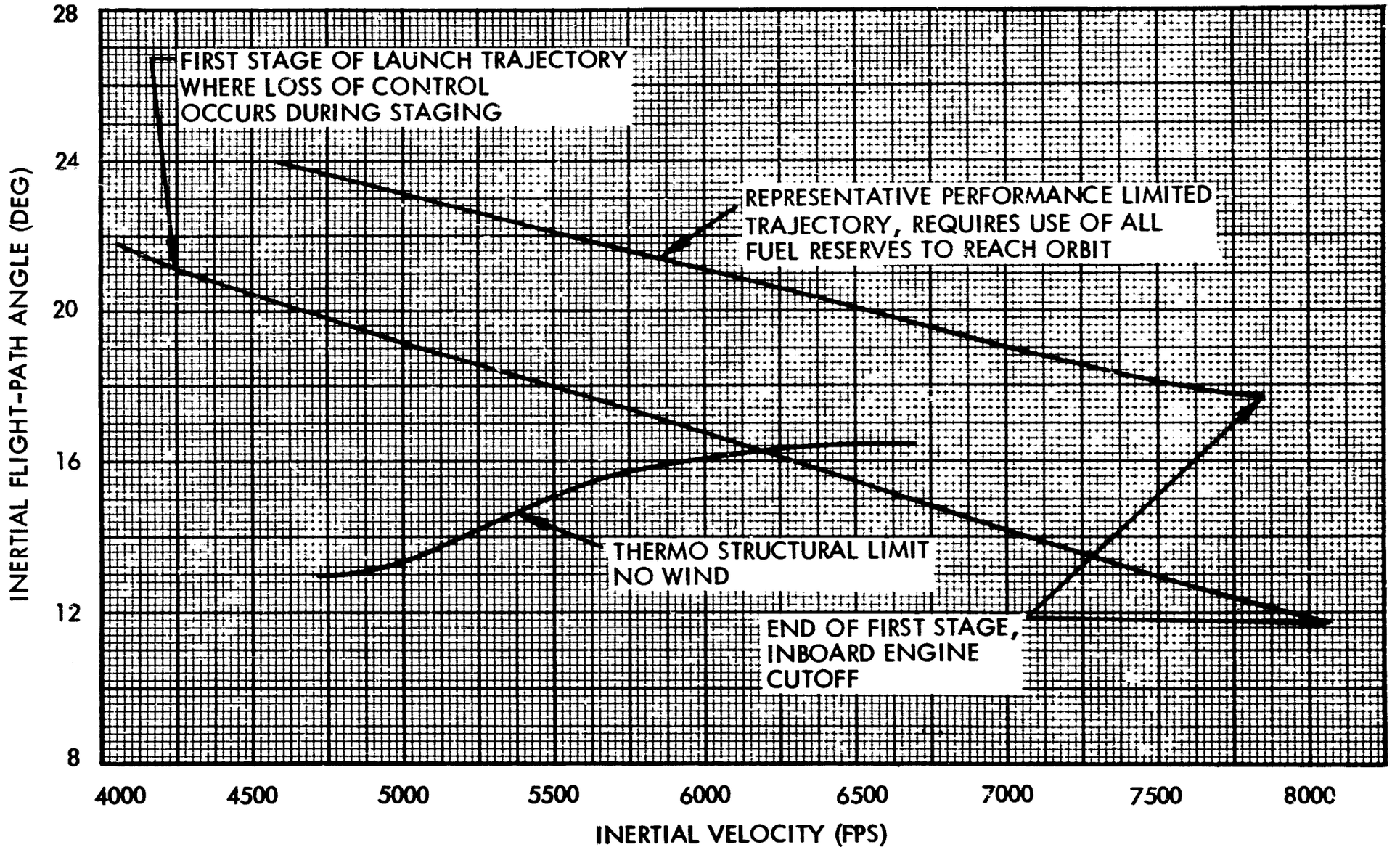


Figure 4-1. Relationship Between Thermo-Structural Limits and Limiting Conditions to Attain Orbit

# REFERENCES


1. J. R. Vail, "Abort Limit Lines Due to Saturn IB and Apollo Block I Structural Constraints," TRW 05952-6082-R0-00, 9 December 1966.

2. TRW Report, "Ascent Heating Program - Users Manual" to be published.

3. T. Ishimoto, "TRW Thermal Analyzer Program Users Manual, Part I, Analytical Development," TRW IOC 66-3331.6-5, 1 April 1966.

4. D. W. Wolsefer, et al., "Aerodynamic Heating to a Thin Skin or Honeycomb Panel," Chrysler Corporation, Space Division, Technical Note TN-AE-64-53, 15 September 1964.

5. A. Gillies, "Apollo CSM-SLA Local Flow Properties," TRW IOC 67.3302.9-1, 27 February 1967.

6. E. R. G. Eckert, "Engineering Relations for Heat Transfer and Friction in High Velocity Laminar and Turbulent Boundary - Layer Flow Over Surfaces With Constant Pressure and Temperature," Transactions of the ASME, pp. 1273-1283, August 1956.

7. E. R. Van Driest, "Turbulent Boundary Layer in Compressible Fluids," Journal of the Aeronautical Sciences, Vol. 18, pp. 145-169, March 1951.

8. SID 66-626, "Apollo Combined Module Static Tests C/M and SM, S/C 004 - Ultimate Loads," North American Aviation, Inc., May 1966.

9. Telcom, P. D. Smith NASA/MSC and C. D. Faust TRW, "Failure of SM Aft Bulkhead during the SC-004 Static Test," 31 March 1967.

10. Mil-HDBK-5A, "Metallic Materials and Elements for Aerospace Vehicle Structures," 8 February 1966.

11. "Full Scale Structural Static Test Spacecraft LEM Adapter (SLA-2), With Structure Stabilizing Device or LEM Test Article (LTA-10)," NAA SID 66T-90, 29 September 1966.

12. NAA, "Contract NAS 9-150, R&D for Project Apollo Spacecraft SM RCS Engine Boost Heating Temperatures," North American Aviation Letter, 66 MA 4257, 25 March 1966.